nature materials

ARTICLES

PUBLISHED ONLINE: 8 DECEMBER 2013 | DOI: 10.1038/NMAT3824

Semi-metallic polymers

Olga Bubnova[1], Zia Ullah Khan[1], Hui Wang[1], Slawomir Braun[2], Drew R. Evans[3], Manrico Fabretto[3], Pejman Hojati-Talemi[3], Daniel Dagnelund[2], Jean-Baptiste Arlin[4], Yves H. Geerts[4], Simon Desbief[5], Dag W. Breiby[6], Jens W. Andreasen[7], Roberto Lazzaroni[5], Weimin M. Chen[2], Igor Zozoulenko[1], Mats Fahlman[2], Peter J. Murphy[3], Magnus Berggren[1] and Xavier Crispin[1]*

Polymers are lightweight, flexible, solution-processable materials that are promising for low-cost printed electronics as well as for mass-produced and large-area applications. Previous studies demonstrated that they can possess insulating, semiconducting or metallic properties; here we report that polymers can also be semi-metallic. Semi-metals, exemplified by bismuth, graphite and telluride alloys, have no energy bandgap and a very low density of states at the Fermi level. Furthermore, they typically have a higher Seebeck coefficient and lower thermal conductivities compared with metals, thus being suitable for thermoelectric applications. We measure the thermoelectric properties of various poly(3,4-ethylenedioxythiophene) samples, and observe a marked increase in the Seebeck coefficient when the electrical conductivity is enhanced through molecular organization. This initiates the transition from a Fermi glass to a semi-metal. The high Seebeck value, the metallic conductivity at room temperature and the absence of unpaired electron spins makes polymer semi-metals attractive for thermoelectrics and spintronics.

Conducting polymers constitute a unique class of materials capable of exhibiting semiconducting and, in some cases, metallic behaviour. The resulting electrical conductivity may vary considerably subject to their oxidation level, chain alignment, interchain interactions, conjugation length, degree of disorder and so on. In the late 1970s copper-like electrical conductivities were reported in polyacetylene films[1]. The discovery of a soluble and highly conducting form of polyaniline showing some degree of self-organization led to the first air-stable and solution-processable metallic polymers[2,3]. The electrical conductivity σ increases when cooling down from room temperature and reaches a finite value at 0 K. Aside from these examples, most of the conducting polymers are semiconductors at room temperature as characterized by the monotonic decrease in σ as $T \rightarrow 0$. This particular case is well described within the Fermi-glass limit as defined by the Anderson localization[4]. The doping charges do not form extended Bloch energy bands but rather occupy localized states associated with a high degree of local atomic and electronic polarization. Concurrently, in the presence of high disorder, the Fermi level E_F is located within the localized states and transport of charge is governed by temperature-activated hopping[5].

Today, various conducting polymers routinely reach σ above 1,500 S cm^{-1}, such as polyaniline[6], polypyrrole[7] and poly(3,4-ethylenedioxythiophene) (PEDOT; ref. 8). Recently, further improvements have been achieved in PEDOT–polystyrene sulphonate (PSS) with an ionic liquid additive (2,000 S cm^{-1}; ref. 9) and an acidic treatment (2,500 S cm^{-1}; ref. 10). The record conductivity value of 3,400 S cm^{-1} was measured in vapour-phase polymerized (VPP) PEDOT–Tos, where Tos represents the counterion tosylate, using a blend of an oxidant and an amphiphilic copolymer[11]. Besides transparent electrodes in optoelectronics, numerous new potential applications are emerging. The thermoelectric properties of PEDOT have been optimized through a control of the oxidation level[12]; as well as through treatment with high-boiling-point solvents leading to a thermoelectric figure-of-merit equal to $ZT = 0.42$ at room temperature[13,14]. These recent breakthroughs bring conducting polymers as attractive low-cost, solution-processable and abundant thermoelectric materials compared with the best inorganic bismuth antimony telluride alloys for low-temperature applications[15]. Recently, PEDOT has made its entry in spintronics. An efficient spin-to-charge conversion was demonstrated between a ferromagnetic insulator and PEDOT. Interestingly, the injected spins have a long lifetime, which is essential to manipulate spins in devices[16]. Yet, no fundamental explanation has been provided for the high thermoelectric efficiencies and long spin lifetimes in conducting polymers. This motivates a deeper understanding of their electronic structure and morphology.

The conducting polymer chains dissolved in solution show clear modification of their optical properties when their oxidation state is modified[17]. The removal of electrons from the top of the valence band in a single polymer chain can lead to two different localized positively charged defects: positive polarons (radical cation) and bipolarons (dication) balanced by atomic or molecular counterions. The change in bond length alternation around the excess of positive charge defines the extent of the wavefunction of the (bi)polaron[18]. This local structural distortion leads to two new in-gap states (i, i*), among which a localized level destabilized from the top of the valence band[18,19]. For a polaron, this level 'i' is half-filled (Fig. 1a), whereas for a bipolaron, it is empty (Fig. 1d). Each of those doping species possesses distinct optical transitions[17,18]. A bipolaron has no spin, whereas a polaron possesses a spin of 1/2 and can be detected by electron spin resonance[20].

[1]Linkoping University, Department of Science and Technology, Organic Electronics, SE-601 74 Norrkoping, Sweden, [2]Linköping University, Department of Physics, Chemistry and Biology, S-581 83 Linköping, Sweden, [3]University of South Australia, Mawson Institute, Mawson Lakes 5095, Australia, [4]Free University of Brussels, Laboratoire de Chimie des Polymères, CP 206/1, Boulevard du Triomphe, 1050 Bruxelles, Belgium, [5]University of Mons, Laboratoire de chimie des materiaux nouveaux, Place du Parc 20, 7000 Mons, Belgium, [6]Norwegian University of Science and Technology (NTNU), Department of Physics, Høgskoleringen 5, 7491 Trondheim, Norway, [7]Technical University of Denmark, Department of Energy Conversion and Storage, Frederiksborgvej 399, 4000 Roskilde, Denmark. *e-mail: xavcr@itn.liu.se

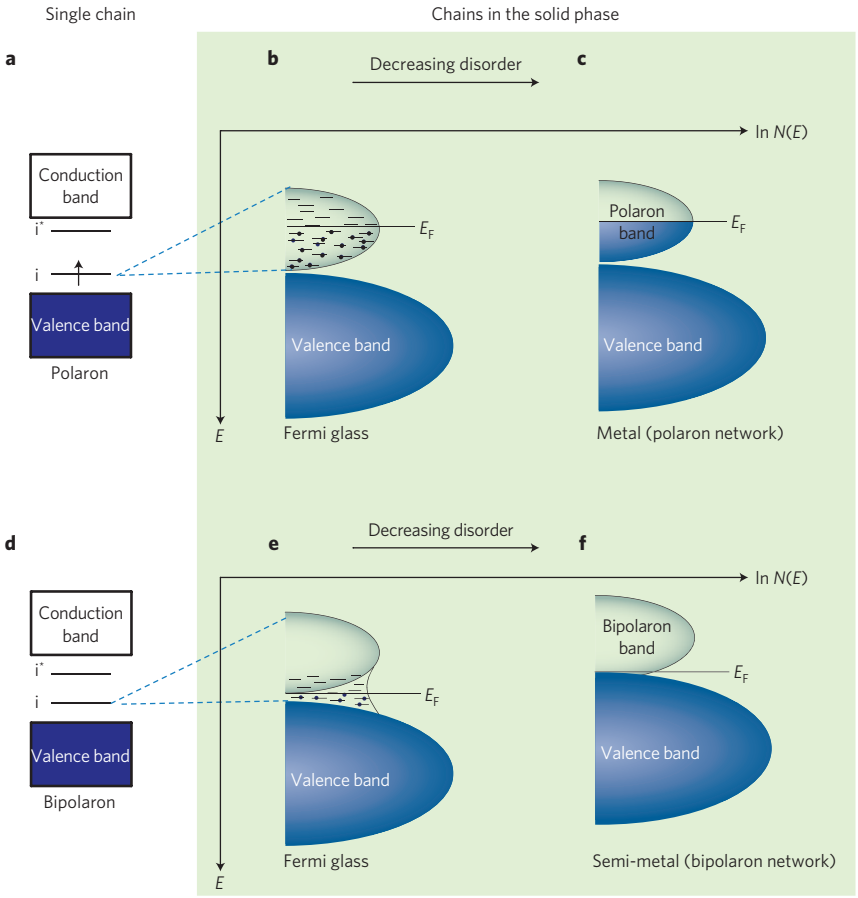

Figure 1 | Electronic structure of conducting polymers. a–c, Case for polarons: electronic structure of a polymer chain with one polaron (**a**), sketch of the logarithm of the DOS ln$N(E)$ for an amorphous polaronic polymer solid with localized states around the Fermi level E_F (**b**), as well as for a metallic network of polarons with the Fermi level lying in a delocalized polaron band (**c**). **d–f**, Case for bipolarons: electronic structure of a polymer chain with one bipolaron (**d**), ln$N(E)$ for an amorphous bipolaronic polymer solid (**e**), as well as for a semi-metallic network of bipolarons with the Fermi level lying between the valence band and the empty bipolaron band (**f**). In the electronic structures, i and i* represent the in-gap states induced by local structural distortions.

In the solid state, the polymer chains arrange either in a disorder fashion or self-organize in crystalline domains[21]. In an amorphous phase, polaron or bipolaron levels are localized on a segment of the chains. At high oxidation levels, the wavefunction of the charged defects localized on the same chain overlap and a one-dimensional 'intra-chain' band is created[22]. However, this band does not extend through the three dimensions of the solid owing to disorder and the absence of the inter-chain electronic coupling[23]. For this reason, in-gap states are spatially localized and spread on an energy distribution. The Fermi level lies among localized states in the middle of the polaron band for a disordered polaronic polymer solid (Fig. 1b); or between the valence band and the bipolaron band for a disordered bipolaronic polymer solid[24] (Fig. 1e). Both solids can be considered as Fermi glasses[25,26]. In crystalline domains of polymers and in molecular crystals, short inter-chain distances result in an overlap of the π-electronic density of adjacent packed chains, which promotes the delocalization of the electronic wavefunction[27], such as a polaron spreads over several chains[28]. Highly oxidized polyaniline can be a metal[2] characterized with a half-filled polaron band originating from the creation of a polaron network (Fig. 1c)[29]. In a first approximation, the slope of the density of states (DOS) at E_F is related to the Seebeck coefficient S (ref. 30). As the Fermi level is in the middle of a band, metals as well as highly oxidized polyaniline have low thermopower ($S < 10\,\mu V\,K^{-1}$; ref. 31). When the degree of disorder decreases, polaronic polymers, such as polyaniline, are known to undergo a transition from Fermi glass to metal[32]. As far as bipolarons are concerned, the situation is unclear. In contrast to polyaniline, polythiophenes such as PEDOT are known to exibit bipolaron defects such as bipolarons[33]. Highly oxidized PEDOT possesses up to one charge carrier per three monomer units[34]. From quantum chemical calculations, a bipolaron in PEDOT spreads over six monomer units or more[35]. However, no clear picture of the band structure is proposed for semi-crystalline bipolaronic polymers and none has demonstrated the possibility to create a network of bipolarons in a polymer solid. Herein, we demonstrate metallic transport at room temperature in a bipolaron network created in polycrystalline PEDOT. In contrast to metals and metallic polyaniline, we measure a large S in PEDOT indicating its semi-metallic character.

PEDOT samples with different σ spreading over six orders of magnitude are prepared. The PEDOT–PSS films are obtained by drop-casting PEDOT–PSS water emulsions to which diethylene glycol (DEG) is added in different amounts[36]. The room temperature σ is $\sim$0.007 S cm^{-1}, $\sim$0.02 S cm^{-1}, $\sim$1.1 S cm^{-1} and $\sim$10 S cm^{-1} for PEDOT–PSS with 0%, 0.05%, 0.5% and 5% DEG respectively. DEG, as well as many other polar solvents, enhances the electrical conductivity through a morphology change[37,38] or a modification in the chain packing[39] (Supplementary Fig. 1), with no effect on the oxidation level (Supplementary Fig. 2). An electrical conductivity of 500 S cm^{-1} is measured in PEDOT with the Tos counterion. PEDOT–Tos is prepared by chemical polymerization (see Supplementary Information)[40]. To further enhance the conductivity,

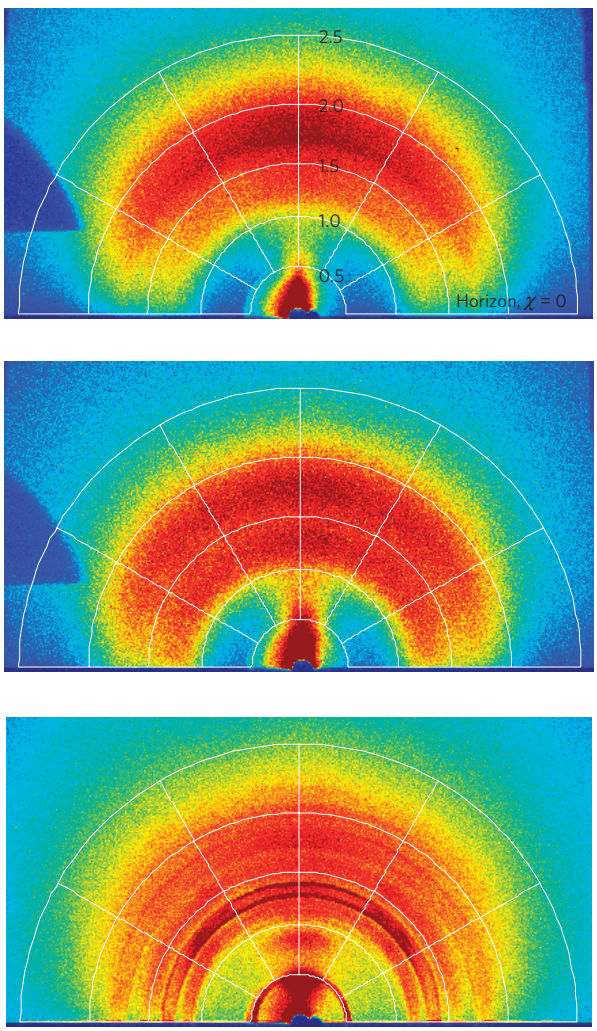

Figure 2 | Structure of various PEDOT thin films. a, GIWAXS patterns obtained for PEDOT–PSS (without DEG), showing mainly a broad peak near $\mathbf{Q} = 1.70\ \text{Å}^{-1}$ ($d \sim 3.7$ Å) that is related to interchain stacking. **b**, PEDOT–PSS 0.05% DEG, showing a broad additional peak at $\mathbf{Q} = 1.25\ \text{Å}^{-1}$ ($d \sim 5.0$ Å) that we ascribe to PSS domains. **c**, PEDOT–Tos, being qualitatively different from the PEDOT–PSS samples with several sharp diffraction rings. The superimposed semicircles give the values for the scattering vector **Q** in units of Å^{-1}, with values as indicated in **a**. The horizon, corresponding to in-plane scattering, is also indicated. The shadow on the left-hand side, seen in **a**,**b** is an experimental artefact.

we use a vapour-phase polymerization technique to fabricate PEDOT–Tos films that are templated by glycol-based triblock copolymers poly(ethylene glycol–propylene glycol–ethylene glycol) (PEG–PPG–PEG; ref. 41). The measured conductivity is 800, 1,200 and 1,500 S cm^{-1} for the copolymer with a molecular weight of 2,900 M_w, 5,800 M_w with dimethylformamide (DMF) as an added solvent, and 5,800 M_w without DMF, respectively.

Grazing incidence wide-angle X-ray scattering (GIWAXS) has become a frequently used tool for the structural characterization of polymers, including PEDOT (refs 39,42–44). GIWAXS patterns for selected PEDOT samples are shown in Fig. 2. All of the PEDOT–PSS samples are essentially amorphous, or 'weakly ordered polymer aggregates'. The broad peak at $\mathbf{Q} \sim 1.70\ \text{Å}^{-1}$ is ascribed to intermolecular ordering of PEDOT chains, presumably involving π-stacking (Fig. 2a). Already with a minor addition of 0.05% DEG to the PEDOT–PSS, another broad peak at $\mathbf{Q} \sim 1.25\ \text{Å}^{-1}$ ($d = 5$ Å) appears (Fig. 2b), possibly originating from separated PSS domains[39]. Some preferred orientation is present in the PEDOT–PSS samples with the π-stacking tending to be out-of-plane. The PEDOT–Tos sample (Fig. 2c) exhibits several sharp diffraction peaks, making this sample qualitatively different from the PEDOT–PSS samples. A likely interpretation of the scattering pattern is that the material contains well-ordered crystallites separated from each other by a less-ordered 'amorphous' matrix. The orthorhombic unit cell suggested for PEDOT–Tos with $a = 14.0$ Å, $b = 6.8$ Å and $c = 7.8$ Å (ref. 45), having the polymer chains parallel to the c axis, accounts fairly well for the experimental peak positions when assuming that the unit cell is oriented (full-width at half-maximum $< 10°$) with the a axis perpendicular to the substrate. This model indicates the formation of lamellae of π-stacked PEDOT chains separated by an inter-lamella space occupied by Tos (refs 39,42). However, the experimental scattering pattern shows pronounced off-axis scattering (at $\chi \sim 40°$ with respect to the substrate plane) with high intensity at the corresponding 201 ($\mathbf{Q} = 1.21\ \text{Å}^{-1}$) and 210 ($\mathbf{Q} = 1.29\ \text{Å}^{-1}$) Bragg peaks that cannot be explained by this model, suggesting that the ribbon-shaped polymer chains in the present case are not fully edge-on with respect to the substrate plane.

The density of valence electronic states (DOVS) can be probed by ultraviolet photoelectron spectroscopy (UPS). The UPS spectra of PEDOT–PSS 5%DEG and PEDOT–Tos are shown in Fig. 3a,b. Close to E_F, the UPS spectrum of PEDOT–PSS shows an abrupt decay at 1.5 eV followed by a smooth tail reaching E_F. Only π-electrons contribute to the signal in that binding energy range. This tail is associated with the presence of localized filled states induced by disorder. The amorphous PEDOT–PSS is a Fermi glass. The PEDOT–Tos UPS spectrum exhibits a large DOVS at E_F and a totally different shape without a disorder-induced tail. PEDOT–Tos with a lower workfunction (4.3 eV) as compared with PEDOT–PSS (5.1 eV) has the valence band closer to E_F. A significant background absorption in the infrared is recorded for PEDOT–Tos (see Supplementary Fig. 2) down to <0.05 eV, implying a vanishingly small bandgap well below the resolution of the photoelectron spectrometer.

Electron paramagnetic resonance spectroscopy (EPR) detects the presence of unpaired electrons in solids[46]. The EPR spectra for the various PEDOT samples are depicted in Fig. 3c. The addition of the secondary dopant, which leads to an increase in σ, systematically diminishes the paramagnetic signal. In PEDOT–PSS, the fraction of spin per monomer equals 2.3% (3.27×10^{16} spin mm^{-3}), 2.2, 1.2 and 0.33% for PEDOT–PSS with 0%, 0.05%, 0.5% and 5% DEG, respectively. On the basis of a carrier density of about 33% per monomer[34,46,47], PEDOT–PSS contains 7% of polarons and 93% bipolarons. The ratio depends on DEG, which probably promotes the pairing of polarons into bipolarons. The remaining EPR signal is intrinsically related to the molecular disorder that impedes the coupling of the remaining polarons to other charged defects. Surprisingly, the polycrystalline PEDOT–Tos shows no ESR signal at all, indicating that polaron pairs[35] or bipolarons are the only type of charge carriers.

The Seebeck coefficient S versus electrical conductivity σ is reported for various PEDOT samples at 300 K (Fig. 4a). For the sake of comparison, S and σ are also reported for a nanostructured BiSbTe alloy[15]. Two main trends can be distinguished: S is almost constant for all PEDOT–PSS samples despite the large variation in σ; S increases markedly for highly conducting PEDOT–Tos samples up to 55 $\mu\text{V K}^{-1}$ for 1,500 S cm^{-1}. This cannot be attributed to different doping levels (see Supplementary Information), as it would lead to an opposite behaviour (large S–low σ; refs 12,48). Interestingly, σ versus T (Fig. 4b) indicates two regimes as well: a semiconducting behaviour with positive temperature coefficient, that is, a thermally activated transport for PEDOT–PSS; and a metallic behaviour for PEDOT–Tos with a negative temperature coefficient at room temperature, which was previously observed only below 10 K (ref. 45). Hence, the regime of charge transport

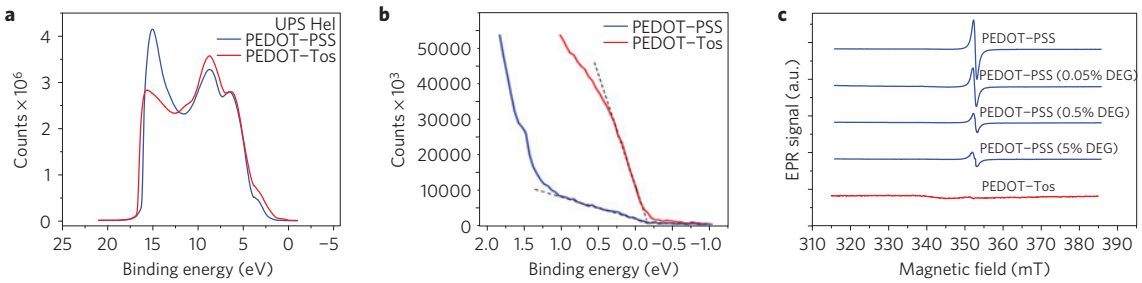

Figure 3 | Electronic valence levels and nature of the charge carriers. a, UPS valence band spectra (HeI radiation) of PEDOT–PSS and PEDOT–Tos. **b**, The magnified view of the low-binding-energy region shows the DOVS of PEDOT–PSS and PEDOT–Tos. The dashed lines are a guide to the eyes for the slope of the DOVS at the Fermi level. A difference in slope implies a difference in Seebeck coefficient. **c**, EPR spectra of untreated (strongest signal) and DEG-treated PEDOT–PSS films; PEDOT–Tos shows no EPR signal.

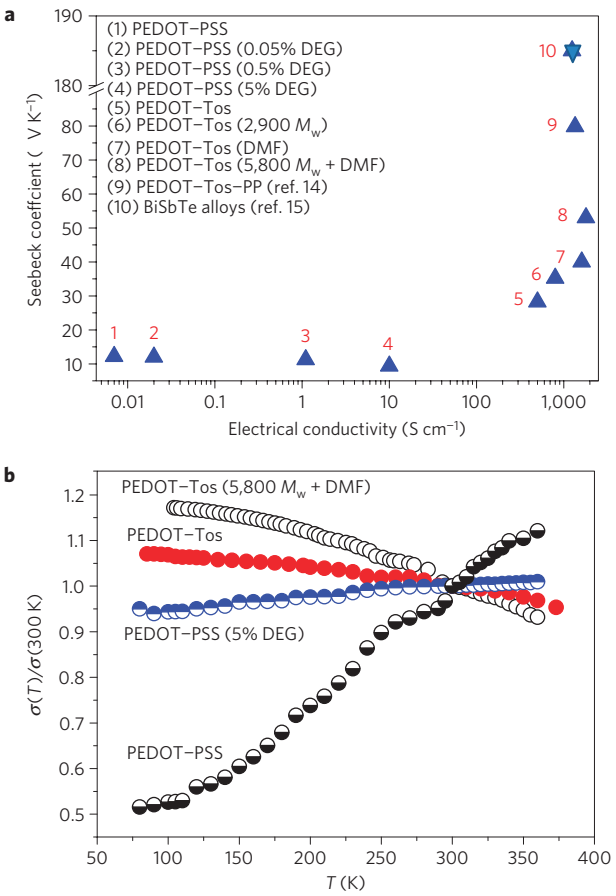

Figure 4 | Thermopower and electrical conductivity of PEDOT derivatives. **a**, Seebeck coefficient versus electrical conductivity of various PEDOT derivatives including pristine PEDOT–PSS and DEG-containing samples, chemically polymerized PEDOT–Tos as well as three VPP PEDOT–Tos samples with triblock copolymers PEG–PPG–PEG with different M_w. Seebeck coefficient for points 9 and 10 is measured using a different set-up. The thermoelectric properties of a BiSbTe alloy (star) is compared with PEDOT derivatives (triangles). **b**, Temperature dependence of the electrical conductivity (normalized to 300 K) for various PEDOT–Tos and PEDOT–PSS samples.

and the value of the Seebeck coefficient show an unexpected correlation. The difference in slope for the metallic σ versus T for the various PEDOT–Tos samples indicates that two modes of transport are active simultaneously with different weights: metallic and hopping conductions. The larger the metallic contribution, the higher the conductivity and, surprisingly, the same applies to the Seebeck coefficient. The large S of PEDOT–Tos as compared with polyaniline ($<10\,\mu V\,K^{-1}$) and other metals suggests that it is not a metal but a semi-metal. We therefore propose that the electronic structure of PEDOT–PSS can be described by a Fermi glass as indicated in Fig. 1e, whereas PEDOT–Tos is defined by what looks more like a bipolaron network with an empty delocalized bipolaron band merging into the delocalized valence band (see Fig. 1f).

With this model in mind, we come back to the interpretation of the S evolution (Fig. 1a). Mott's formula[49], which is valid for both hopping and band motion transport mechanisms, states that S is proportional to $[d(\ln\sigma(E))/dE]$ at E_F. As the energy dependence of the conductivity is primarily determined by the DOS $N(E)$ (for details see Supplementary Information), the Seebeck coefficient is therefore proportional to $[d(\ln N(E))/dE]_{E=E_F}$. In the amorphous bipolaron system (Fig. 1e), E_F lies in the localized states fading out from the valence and bipolaron bands. As supported by the UPS data, the DOS at E_F is not varying much and is close to its minimum, which explains the low value of S of PEDOT–PSS. For PEDOT–Tos, E_F is in a strongly varying DOS region (Fig. 1f), such that $[d(\ln N(E))/dE]_{E=E_F}$ and S are larger. Note that the DOS asymmetry is amplified with structural order as the localized levels smooth out the DOS. This explains the larger S for PEDOT–Tos with high σ. It is clear that further improvement in structural order (higher σ) should in principle result in even larger S and thus thermoelectric power factor σS^2. In disordered or metallic polyaniline with polarons as major doping species, E_F is in a slowly varying region of the DOS (Fig. 1b,c). Hence, conducting polymers composed of a bipolaron network (semi-metallic) are expected to have better thermoelectric properties than those with a polaron network (metallic). Finally, the absence of (residual) polarons in semi-metallic PEDOT–Tos is a unique feature that can be exploited in spintronics, because the absence of unpaired electrons in the solid prevents spin scattering and increases the spin lifetime.

Received 21 May 2013; accepted 30 October 2013; published online 8 December 2013

References

1. Chiang, C. K. *et al.* Electrical conductivity in doped polyacetylene. *Phys. Rev. Lett.* **39,** 1098–1101 (1977).
2. Lee, K. *et al.* Metallic transport in polyaniline. *Nature* **441,** 65–68 (2006).
3. Cao, Y., Treacy, G. M., Smith, P. & Heeger, A. J. Solution-cast films of polyaniline: Optical-quality transparent electrodes. *Appl. Phys. Lett.* **60,** 2711–2713 (1992).
4. Fleishman, L., Licciardello, D. C. & Anderson, P. W. Elementary excitations in the Fermi glass. *Phys. Rev. Lett.* **40,** 1340–1343 (1978).
5. Wang, S., Ha, M., Manno, M., Daniel Frisbie, C. & Leighton, C. Hopping transport and the Hall effect near the insulator–metal transition in electrochemically gated poly(3-hexylthiophene) transistors. *Nature Commun.* **3,** 1210 (2012).
6. Pomfret, S. J., Adams, P. N., Comfort, N. P. & Monkman, A. P. Inherently electrically conductive fibers wet spun from a sulfonic acid–doped polyaniline solution. *Adv. Mater.* **10,** 1351–1353 (1998).

7. Yamaura, M., Hagiwara, T. & Iwata, K. Enhancement of electrical conductivity of polypyrrole film by stretching: Counter ion effect. *Synth. Met.* **26,** 209–225 (1988).
8. Fabretto, M. *et al.* High conductivity PEDOT resulting from glycol/oxidant complex and glycol/polymer intercalation during vacuum vapour phase polymerisation. *Polymer* **52,** 1725–1730 (2011).
9. Badre, C., Marquant, L., Alsayed, A. M. & Hough, L. A. Highly conductive poly(3,4-ethylenedioxythiophene):poly (styrenesulfonate) films using 1-ethyl-3-methylimidazolium tetracyanoborate ionic liquid. *Adv. Funct. Mater.* **22,** 2723–2727 (2012).
10. Xia, Y., Sun, K. & Ouyang, J. Solution–processed metallic conducting polymer films as transparent electrode of optoelectronic devices. *Adv. Mater.* **24,** 2436–2440 (2012).
11. Fabretto, M. V. *et al.* Polymeric material with metal-like conductivity for next generation organic electronic devices. *Chem. Mater.* **24,** 3998–4003 (2012).
12. Bubnova, O. *et al.* Optimization of the thermoelectric figure of merit in the conducting polymer poly(3,4-ethylenedioxythiophene). *Nature Mater.* **10,** 429–433 (2011).
13. Kim, G. H., Shao, L., Zhang, K. & Pipe, K. P. Engineered doping of organic semiconductors for enhanced thermoelectric efficiency. *Nature Mater.* **12,** 719–723 (2013).
14. Park, T., Park, C., Kim, B., Shin, H. & Kim, E. Flexible PEDOT electrodes with large thermoelectric power factors to generate electricity by the touch of fingertips. *Energy Environ. Sci.* **6,** 788–792 (2013).
15. Bed Poudel, Q. H. *et al.* High-thermoelectric performance of nanostructured bismuth antimony telluride bulk alloys. *Science* **320,** 634–638 (2008).
16. Ando, K., Watanabe, S., Mooser, S., Saitoh, E. & Sirringhaus, H. Solution–processed organic spin–charge converter. *Nature Mater.* **12,** 622–627 (2013).
17. Jeuris, K., Groenendaal, L., Verheyen, H., Louwet, F. & De Schryver, F. C. Light stability of 3,4-ethylenedioxythiophene-based derivatives. *Synth. Met.* **132,** 289–295 (2003).
18. Cornil, J., Beljonne, D. & Bredas, J. L. Nature of optical transitions in conjugated oligomers. I. Theoretical characterization of neutral and doped oligo(phenylenevinylene)s. *J. Chem. Phys.* **103,** 834 (1995).
19. Brédas, J. L., Wudl, F. & Heeger, A. J. Polarons and bipolarons in doped polythiophene: A theoretical investigation. *Solid State Commun.* **63,** 577–580 (1987).
20. Devreux, F., Genoud, F., Nechtschein, M. & Villeret, B. ESR investigation of polarons and bipolarons in conducting polymers: The case of polypyrrole. *Synth. Met.* **18,** 89–94 (1987).
21. Martin, D. C. *et al.* The morphology of poly(3,4-ethylenedioxythiophene). *Polym. Rev.* **50,** 340–384 (2010).
22. Stafström, S. & Brédas, J. L. Evolution of the electronic structure of polyacetylene and polythiophene as a function of doping level and lattice conformation. *Phys. Rev. B* **38,** 4180–4191 (1988).
23. Prigodin, V. N. & Efetov, K. B. Localization transition in a random network of metallic wires: A model for highly conducting polymers. *Phys. Rev. Lett.* **70,** 2932–2935 (1993).
24. Lavarda, F. C., dos Santos, M. C., Galvão, D. S. & Laks, B. Insulator-to-metal transition in polythiophene. *Phys. Rev. B* **49,** 979–983 (1994).
25. Sariciftci, N. S., Heeger, A. J. & Cao, Y. Paramagnetic susceptibility of highly conducting polyaniline: Disordered metal with weak electron-electron interactions (Fermi glass). *Phys. Rev. B* **49,** 5988–5992 (1994).
26. Heeger, A. J. Semiconducting and metallic polymers: The fourth generation of polymeric materials (nobel lecture). *Angew. Chem. Int. Ed.* **40,** 2591–2611 (2001).
27. Koller, G. *et al.* Intra- and intermolecular band dispersion in an organic crystal. *Science* **317,** 351–355 (2007).
28. Beljonne, D. *et al.* Optical signature of delocalized polarons in conjugated polymers. *Adv. Funct. Mater.* **11,** 229–234 (2001).
29. Stafström, S. *et al.* Polaron lattice in highly conducting polyaniline: Theoretical and optical studies. *Phys. Rev. Lett.* **59,** 1464–1467 (1987).
30. Snyder, G. J. & Toberer, E. S. Complex thermoelectric materials. *Nature Mater.* **7,** 105–114 (2008).
31. Mateeva, N., Niculescu, H., Schlenoff, J. & Testardi, L. R. Correlation of Seebeck coefficient and electric conductivity in polyaniline and polypyrrole. *J. Appl. Phys.* **83,** 3111–3117 (1998).
32. Yoon, C. O. *et al.* Hopping transport in doped conducting polymers in the insulating regime near the metal-insulator boundary: Polypyrrole, polyaniline and polyalkylthiophenes. *Synth. Met.* **75,** 229–239 (1995).
33. Zykwinska, A., Domagala, W., Czardybon, A., Pilawa, B. & Lapkowski, M. *In situ* EPR spectroelectrochemical studies of paramagnetic centres in poly(3,4-ethylenedioxythiophene) (PEDOT) and poly(3,4-butylenedioxythiophene) (PBuDOT) films. *Chem. Phys.* **292,** 31–45 (2003).
34. Zotti, G. *et al.* Electrochemical and XPS studies toward the role of monomeric and polymeric sulfonate counterions in the synthesis, composition, and properties of poly(3,4-ethylenedioxythiophene). *Macromolecules* **36,** 3337–3344 (2003).
35. Geskin, V. M. & Brédas, J-L. Polaron pair versus bipolaron on oligothiophene chains: A theoretical study of the singlet and triplet states. *ChemPhysChem* **4,** 498–505 (2003).
36. Crispin, X. *et al.* The origin of the high conductivity of poly(3,4-ethylenedioxythiophene)–poly(styrenesulfonate) (PEDOT–PSS) plastic electrodes. *Chem. Mater.* **18,** 4354–4360 (2006).
37. Jonsson, S. K. M. *et al.* The effects of solvents on the morphology and sheet resistance in poly (3,4-ethylenedioxythiophene)–polystyrenesulfonic acid (PEDOT–PSS) films. *Synth. Met.* **139,** 1–10 (2003).
38. Nardes, A. M., Janssen, R. A. J. & Kemerink, M. A morphological model for the solvent-enhanced conductivity of PEDOT:PSS thin films. *Adv. Funct. Mater.* **18,** 865–871 (2008).
39. Kim, B. H. L. N. *et al.* Role of interchain coupling in the metallic state of conducting polymers. *Phys. Rev. Lett.* **109,** 106405 (2012).
40. Winther-Jensen, B. & West, K. Vapor-phase polymerization of 3,4-ethylenedioxythiophene: A route to highly conducting polymer surface layers. *Macromolecules* **37,** 4538–4543 (2004).
41. Evans, D. *et al.* Structure-directed growth of high conductivity PEDOT from liquid-like oxidant layers during vacuum vapor phase polymerization. *J. Mater. Chem.* **22,** 14889–14895 (2012).
42. Winther-Jensen, B. *et al.* Order–disorder transitions in poly(3,4-ethylenedioxythiophene). *Polymer* **49,** 481–497 (2008).
43. Winther-Jensen, B. *et al.* High current density and drift velocity in templated conducting polymers. *Org. Electron.* **8,** 796–800 (2007).
44. Breiby, D. W., Samuelsen, E. J., Groenendaal, L. B. & Struth, B. Smectic structures in electrochemically prepared poly(3,4-ethylenedioxythiophene) films. *J. Polym. Sci. B* **41,** 945–952 (2003).
45. Aasmundtveit, K. E. *et al.* Structure of thin films of poly(3,4-ethylenedioxythiophene). *Synth. Met.* **101,** 561–564 (1999).
46. Domagala, W., Pilawa, B. & Lapkowski, M. Quantitative *in-situ* EPR spectroelectrochemical studies of doping processes in poly(3,4-alkylenedioxythiophene)s: Part 1: PEDOT. *Electrochim. Acta* **53,** 4580–4590 (2008).
47. Crispin, X. *et al.* Conductivity, morphology, interfacial chemistry, and stability of poly(3,4-ethylene dioxythiophene)–poly(styrene sulfonate): A photoelectron spectroscopy study. *J. Polym. Sci. B* **41,** 2561–2583 (2003).
48. Bubnova, O., Berggren, M. & Crispin, X. Tuning the thermoelectric properties of conducting polymers in an electrochemical transistor. *J. Am. Chem. Soc.* **134,** 16456–16459 (2012).
49. Cutler, M. & Mott, N. F. Observation of Anderson localization in an electron gas. *Phys. Rev.* **181,** 1336–1340 (1969).

Acknowledgements

The authors acknowledge the European Research Council (ERC-starting-grant 307596), the Swedish foundation for strategic research (project: 'Nano-material and Scalable TE materials'), the Knut and Alice Wallenberg foundation (project 'Power paper'), The Swedish Energy Agency and the Advanced Functional Materials Center at Linköping University. Research in Mons is supported by the European Commission and Région Wallonne (FEDER 'Revêtements Fonctionnels' programme), BELSPO (IAP 7/05), the OPTI2MAT Excellence program of Région Wallonne, and FNRS-FRFC. Research at the University of South Australia is supported by ITEK, the commercialization company for UniSA. Research at NTNU is supported by the Norwegian Research Council.

Author contributions

O.B., Z.U.K. and H.W.—fabrication of the various PEDOT–PSS samples and some PEDOT–Tos samples; thermoelectric and optical characterization of PEDOT–PSS and PEDOT–Tos samples. S.B. and M.F.—photoelectron spectroscopy characterization. D.R.E., M.F., P.H-T. and P.J.M.—fabrication of the various VPP PEDOT–Tos samples. D.D. and W.M.C.—characterization with electron paramagnetic resonance spectroscopy. J-B.A., Y.H.G., D.W.B. and J.W.A.—polarized microscopy, X-ray diffraction and GIWAXS structure analysis. S.D. and R.L.—atomic force microscopy characterization I.Z., M.B. and X.C.—theoretical insight, interpretation and project leading. All authors have been involved in the redaction of the manuscript.

Additional information

Supplementary information is available in the online version of the paper. Reprints and permissions information is available online at www.nature.com/reprints. Correspondence and requests for materials should be addressed to X.C.

Competing financial interests

The authors declare no competing financial interests.